Ultrafast Dynamics of Electron Localization and Solvation in Ice Layers on Cu(111)

C. Gahl, U. Bovensiepen, C. Frischkorn, and M. Wolf*

Fachbereich Physik, Freie Universität Berlin, Arnimallee 14, 14195 Berlin-Dahlem, Germany

(Received 16 April 2002; published 14 August 2002)

The femtosecond dynamics of localization and solvation of photoinjected electrons in ultrathin layers of amorphous solid H_2O and D_2O have been studied by time- and angle-resolved two-photon-photoelectron spectroscopy. After electron transfer from the metal substrate into the conduction band of ice, the excess electron localizes within the first 100 fs in a state at 2.9 eV above E_F, which is further stabilized by 300 meV on a time scale of 0.5–1 ps due to molecular rearrangements in the adlayer. A pronounced change of the solvation dynamics at a coverage of ~2 bilayers is attributed to different rigidity of the solvation shell in the bulk and near the surface of ice.

DOI: 10.1103/PhysRevLett.89.107402 PACS numbers: 78.47.+p, 73.90.+f, 79.60.Dp

The dynamics of excess electrons in water have attracted widespread interest due to the fundamental importance of solvation and charge-transfer processes in physics, chemistry, and biology [1–6]. Water, as a polar solvent, can stabilize an excess electron. In equilibrium, this hydrated electron is localized in a cavity with a radius of ~3 Å [7] surrounded by a solvation shell of ~6 molecules [7–9]. Using ultrafast laser spectroscopy, the dynamics of the generation of solvated electrons in liquid water and its excited states have been investigated in growing detail during the past decade [2–5]. Upon photoexcitation the excess electron is created in an extended state, localizes in a preexisting trap formed by solvent fluctuations, and relaxes via several precursor states to the fully equilibrated ground state within 0.5–1 ps. These rich dynamics are governed by ultrafast librational and slower translational motions of the solvation shell [4,6].

Up to now, most studies have focused on the solvation dynamics in the liquid phase, but very little is known about the initial stages of electron transfer and solvation of excess electrons in supercooled water and ice [10]. However, this knowledge is important for such diverse areas like astrophysics, environmental science, and radiation chemistry. For example, photoinjection of electrons into amorphous ice films was demonstrated to induce molecular rearrangements and nonthermal crystallization of ice [11]. Electrons trapped in precursor states to solvated electrons in ice are known to strongly enhance the dissociation rate of chlorofluorocarbons adsorbed on ice surfaces, a reaction which is of high relevance in the depletion of the ozone layer by released Cl atoms from stratospheric clouds [12].

In this Letter, we investigate the ultrafast dynamics upon electron injection from a metal surface into ultrathin layers of amorphous ice using angle- and time-resolved two-photon-photoelectron (2PPE) spectroscopy. In contrast to optical spectroscopy, 2PPE provides access to absolute values of binding energies and wave vectors, $k_{||}$, parallel to the surface, which yields information about the degree of localization. We have succeeded in separating all elementary processes following electron transfer from the metal into the ice layer. It leads to ultrafast relaxation in extended conduction band states and buildup of a localized solvated electron state within 100 fs. The dynamics of solvation are observed directly through a transient increase of the electron binding energy within ~1 ps competing with the population decay due to back transfer to the metal. Moreover, a pronounced dependence on the ice coverage enables us to study the structural influence on the dynamics of the solvation shell in the condensed phase.

Ice layers are grown in ultrahigh vacuum by expanding H_2O (D_2O) through a pinhole onto a cold Cu(111) crystal at 100 K, which is prepared by standard procedures [13]. The water coverage Θ is determined from thermal desorption spectra (TDS), which are routinely taken after 2PPE experiments. Θ is calibrated with respect to the TDS from the ordered $(\sqrt{3} \times \sqrt{3})$ bilayer structure (1 BL) of D_2O/Ru(0001) [14]. Water deposited below 140 K is known to form an amorphous solid [15]. However, scanning tunneling microscopy reveals a layer-by-layer growth for $\Theta \geq 3$ BL [16]. Crystalline ice layers are prepared by annealing the sample up to 155 K [11,15]. For the time-resolved 2PPE experiments [13] a frequency-doubled pulse $h\nu_1$ and its time-delayed visible fundamental ($h\nu_2$ = 1.7 to 2.7 eV) serve as pump and probe with 65 fs pulse length each. Except for dispersion measurements, photoemitted electrons are detected along the surface normal by a time-of-flight spectrometer.

Time-resolved 2PPE spectra at normal emission from amorphous ice layers on Cu(111) are plotted in Fig. 1 as a function of the intermediate state energy $E - E_F = E_{\text{kin}} + \Phi - h\nu_2$ (see inset). For 4 BL D_2O (panel a) two water induced features are observed: (i) A broad structureless continuum e_{CB} between 3.0 and 3.8 eV decays rapidly within the pulse duration. (ii) A pronounced peak e_S at 2.9 eV shifts to lower energy and increases its asymmetry with time. At lower Θ [Fig. 1(b) for Θ = 1 BL], e_S and e_{CB} are also visible, but the peak e_S shifts considerably faster than for 4 BL. In addition, the surface state (SS) and the first image potential state (IS) of the bare Cu(111) surface [17] are observed, which overlap with e_{CB}. In Fig. 2, the temporal shift of the peak maximum of e_S is depicted for

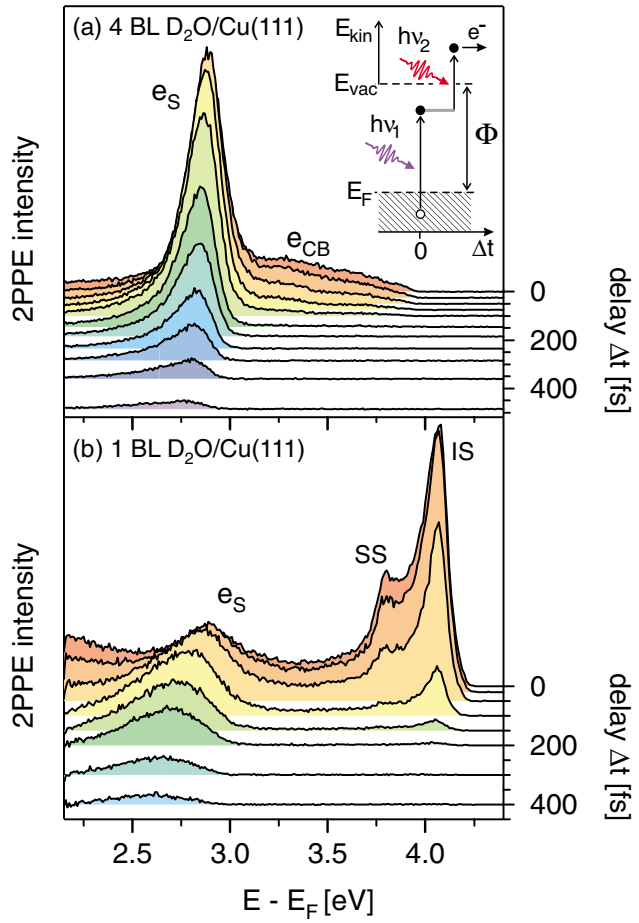

FIG. 1 (color online). Time-resolved 2PPE spectra at normal emission of (a) 4 BL D_2O/Cu(111) at $h\nu_1 = 3.90$ eV, $h\nu_2 = 1.95$ eV, and of (b) 1 BL at $h\nu_1 = 4.20$ eV, $h\nu_2 = 2.10$ eV; Φ denotes the work function. e_{CB} and e_S originate from the water conduction band and the solvated electron, respectively.

different Θ. Two distinct regimes are identified: For high Θ (3–5 BL, solid symbols), a quasilinear peak shift of 270 meV/ps is found. At low $\Theta < 2$ BL (open symbols), the shift is about 4 times faster for $\Delta t < 300$ fs. Very similar results are observed for H_2O (not shown). The inset in Fig. 2 depicts pump-probe measurements for $\Theta = 4$ BL. The population of e_{CB} (•) decays rapidly within the pulse width, while e_S (∘) decays nonexponentially and is observed up to 1.4 ps. Almost identical results were obtained at $\Delta t < 1$ ps for crystalline ice layers, where, however, long-lived electrons lead to signal accumulation of several laser pulses. In the following, we focus on high coverages $\Theta > 2$ BL of amorphous ice. The coverage dependence of the solvation dynamics will be addressed further below.

Stabilization of an excess electron by a solvent shell requires localization of the electronic wave function. In order to test the localized character of peak e_S, we have carried out angle-resolved measurements, which are displayed in Fig. 3 for $\Theta = 3$ BL. The peak positions are evaluated by the first moment of the spectra to account for

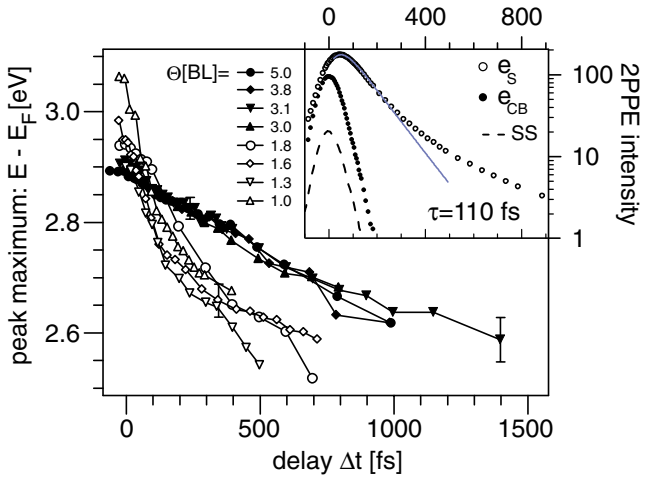

FIG. 2 (color online). Temporal evolution of the peak maximum of e_S for different Θ of D_2O/Cu(111). The inset shows the integrated 2PPE intensities of e_S and e_{CB} versus Δt. An exponential decay fits e_S up to 200 fs with $\tau = 110$ fs (solid line). The dashed line depicts the 2PPE intensity of the surface state on Cu(111), which characterizes the pulse width [17].

the asymmetric peak shape and the overlap of e_S with e_{CB}. The temporal evolution is depicted in Fig. 3(c): At $\Delta t = 0$ fs the peak disperses to higher energies for increasing $k_{||}$. Within 100 fs the dispersion flattens completely, which indicates the transition from an extended to a

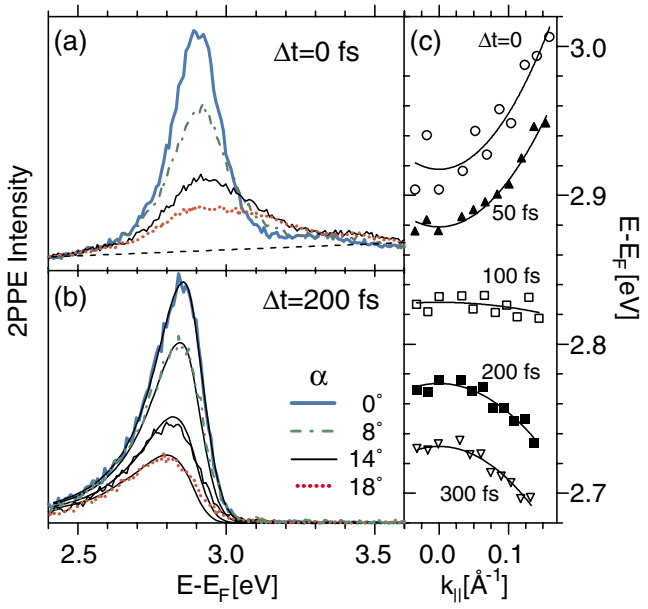

FIG. 3 (color online). Angle-dependent 2PPE spectra for 3 BL D_2O/Cu(111) at (a) 0 fs and (b) 200 fs normalized to their low energy intensity; solid lines are calculated by a model, which yields the width of a wave packet in k space; (c) dispersion $E(k_{||})$ of the first moment of the 2PPE intensity evaluated between 2.4 and 3.6 eV with a linear background subtracted [dashed line in (a)]; solid lines present least square fits of a parabolic function to the data.

localized state [18]. At $\Delta t \geq 100$ fs the peak shifts to lower energy for larger $k_{||}$ and an apparently negative dispersion is found, which—in the present case—is still consistent with a localized state, as discussed below.

We now summarize the experimental results and identify four elementary steps, which are discussed with the help of Fig. 4:

(1) Electron transfer into the conduction band of the ice layer.—With the photon energies available, a direct excitation in the adsorbate from the valence band (VB) to the conduction band (CB) is highly improbable due to the band gap of ice $E_{\text{gap}} = 8.2$ eV [19]. Since no occupied states are available (VB is located > 5 eV below E_F [20]), electrons excited by the pump pulse have to originate from the metal substrate [step (1), Fig. 4]. The good overlap of the delocalized wave functions of the photoexcited metal electrons and the CB, due to its finite penetration depth into the metal, provides efficient charge transfer into the ice CB. This is consistent with the ultrafast decay of the signal e_{CB} caused by electron transfer back to the metal (see inset of Fig. 2). In addition, a positive dispersion is obtained ($\Delta t = 0$ fs in Fig. 3), which corroborates the delocalized nature of the electron wave function after the initial injection step.

(2) Electron localization.—Apart from relaxation back to the substrate, the delocalized electron in the CB can find specific sites in the adlayer which offer favorable molecular configurations for localization. The initially extended electronic wave function localizes at these sites, which are created by, e.g., fluctuations of bond angles or uncompensated hydrogen bonds [21]. The corresponding experimental observation is the pronounced flattening of the dispersion, which occurs within the first 100 fs (Fig. 3). A known process which matches this time scale is the librational response of the immediate molecular environment of the electron [4]. The proposed scheme in Fig. 4 draws an analogy to Marcus' electron transfer reactions [22] and is similar to the model used by Harris and co-workers for electron self-trapping at surfaces [18]: The potentials shown in the right panel describe one-dimensional profiles of the potential energy landscape of the electron in a polar environment reflecting the dependence on various nuclear coordinates q_i. The CB is represented by $V_{CB}(k_{||}, q_1)$ with the unperturbed configuration $q_1^{(0)}$. The manifold of $k_{||}$ and its dispersion within CB are depicted by the filled area. The localization process starts with creating a wave packet of finite width $\Delta k_{||}$ from an initially extended wave function and then proceeds along $V_S(q_1)$, if the resulting stabilization exceeds the localization energy.

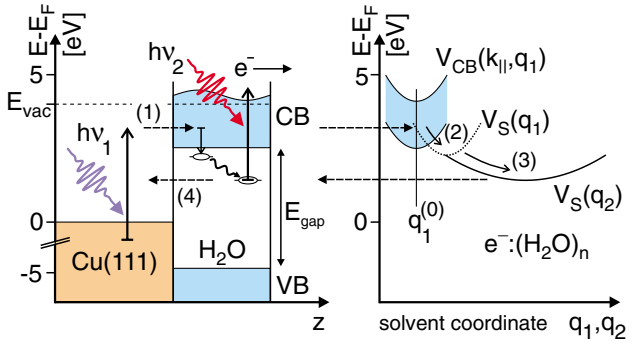

FIG. 4 (color online). Scheme of electron transfer, localization, solvation, and back transfer: The electronic structure is shown on the left, the potentials along the configurational coordinates q_1, q_2 of the solvent on the right; for steps (1)–(4), see text.

(3) Electron solvation.—After the quasi-instantaneous electron injection into the ice layer (time scale ~ 10 fs) and subsequent localization (~ 100 fs), the electron is further stabilized on a picosecond time scale representing an extension to the self-trapping phenomena observed in Ref. [18]. This additional process manifests itself experimentally as a shift in the binding energy (Figs. 1 and 2) and is caused by rearrangement of the water dipoles, a process which is referred to as solvation. Photoreactions as an origin of the peak shift are ruled out, since the change of the work function during a series of experiments is negligible. An intraband relaxation mechanism is also excluded, because it is inconsistent with the localized character of the solvated electron. Further details about the solvation dynamics are obtained from isotopic substitution measurements. Within our experimental time resolution no isotope effect is found, consistent with observations in liquid water [4,6]: Only librational motions are sensitive to deuteration within the first 20 fs, whereas translational/diffusive motions occurring on a longer time scale exhibit no isotope effect.

Qualitatively, as seen in the potential diagram of Fig. 4, solvation leading to an $e^-:(H_2O)_n$ complex evolves on the potential V_S along q_2, a solvent coordinate different from q_1. It proceeds on a time scale of several 100 fs (Fig. 2), hence more slowly than the initial localization along q_1, which in turn can be regarded as the first part of the entire solvation process. However, signal decay [see step (4) below] in conjunction with the finite energy interval probed with 2PPE due to the cutoff at E_{vac} prevent the shift from being observed beyond ~ 1.4 ps, where solvated electrons are still equilibrating.

Localization and solvation confine the wave function of the originally delocalized electron. In order to extract information about this confinement, we analyze the angle-resolved spectra of Fig. 3, whose apparently negative dispersion $\Delta t \geq 100$ fs was not yet addressed. First, we exclude final state effects in the water CB as origin for this behavior, because at early times a positive dispersion is found. For extended states in the CB, $k_{||}$ is a valid concept. The shallow potential well of the solvated electron presents a weak local perturbation of the CB. Since the resulting change of $k_{||}$ is small, we propose the following model [23]: We consider a localized state with spatial width Δx corresponding to a Gaussian distribution of $k_{||}$ with width $\Delta k_{||}$. The measured 2PPE spectrum at $k_{||} = 0$ is weighted

by this $k_{||}$ distribution in order to calculate the 2PPE spectra at different emission angles. For a $\Delta k_{||}$ which increases linearly with decreasing energy, we obtain a perfect agreement as seen in Fig. 3(b). This suggests that the solvated electron is more confined for higher binding energy. By $\Delta x \Delta k_{||} \geq 1$ the spatial extent of the local disturbance of the final electronic state is estimated to be 15–25 Å. This is consistent with the nonequilibrium character of e_S, if compared to 3 Å of the equilibrated case in liquid water [7].

(4) Electron transfer back to the metal.—At all times during steps (1) to (3) following the primary photoexcitation, relaxation processes allow electron transfer back to the Cu substrate. The crucial parameter is the wave function overlap of the initial and final states. Even electrons which survive all the way to the formation of the solvated complex $e^-:(H_2O)_n$ finally transfer back to the metal, as seen by the decay of signal e_S (Fig. 2, inset). The pronounced nonexponential decay after ~200 fs supports the proposed energy dependence of the degree of confinement. Increasing localization of the electronic wave packet reduces the coupling with metal states and thus the rate of back transfer to the substrate.

Finally, we address the intriguing question of how the coverage and hence the structure of the adlayer influence the solvation dynamics. The peak shifts in Fig. 2 exhibit two distinct coverage regimes. For $\Theta \leq 2$ BL, the energy shift occurs much faster than for larger coverages $\Theta \geq 3$ BL. This allows to draw conclusions on the local molecular structure in the vicinity of the solvated electron. In the high coverage regime, the solvation dynamics are not affected by additional layers as expected for solvation in the bulk. Contrary to that, at lower Θ, an electron trapped near the surface of the ice layer is stabilized more readily and hence faster, since the lower coordination of molecules causes a less rigid network of the solvent dipoles with respect to bulk. Although we cannot exclude surface states as discussed for gas-phase clusters [24], the electron binding energies should be smaller, because fewer molecules contribute to the solvation.

From the presence of the image potential state of Cu(111) in Fig. 1(b) at a D_2O coverage of 1 BL we conclude that at low coverage three-dimensional islands coexist with areas of bare Cu surface. This behavior is found for $\Theta \leq 2$ BL. Since STM images a flat surface for $\Theta \geq 3$ BL [16], the coalescence of patches occurs between 2 and 3 BL. This coverage coincides with the transition in the dynamics at 2–3 BL (Fig. 2), which emphasizes the sensitivity of the solvation process to the structure of the solvent. Our results thus demonstrate the possibility to investigate the relation between structure and solvation dynamics in low dimensional systems. Adsorption on solid surfaces is a promising approach, because variation of the substrate, which serves as a template, facilitates systematic variation of the solvent structure.

In summary, we have time-resolved the elementary steps of electron solvation in amorphous ice layers on a metal surface. Photoinjection of excess electrons in the water conduction band is followed by electron localization and subsequent solvation caused by rearrangement of the surrounding water dipoles. A systematic coverage variation reveals a pronounced dependence of the solvation on the structure of the ice. Since the electron dynamics at the ice-metal interface can be regarded as a model system, our study has general implications for the understanding of charge-transfer reactions at interfaces even in photocatalysis and electrochemistry.

We thank G. Ertl for supporting the experiments at the Fritz-Haber-Institut der MPG. Valuable discussions with K. Horn, A. Hotzel, and P. Vöhringer and funding by the Deutsche Forschungsgemeinschaft are acknowledged.

*Email address: wolf@physik.fu-berlin.de
Electronic address: http://www.physik.fu-berlin.de/~femtoweb

[1] A. Migus *et al.*, Phys. Rev. Lett. **58**, 1559 (1987).
[2] F. H. Long, H. Lu, and K. B. Eisenthal, Phys. Rev. Lett. **64**, 1469 (1990).
[3] C. Silva *et al.*, Phys. Rev. Lett. **80**, 1086 (1998).
[4] M. F. Emde *et al.*, Phys. Rev. Lett. **80**, 4645 (1998).
[5] R. Laenen, T. Roth, and A. Laubereau, Phys. Rev. Lett. **85**, 50 (2000).
[6] C.-Y. Yang *et al.*, J. Chem. Phys. **114**, 3598 (2001).
[7] T. W. Kee *et al.*, J. Phys. Chem. A **105**, 8434 (2001).
[8] L. Kevan, Acc. Chem. Res. **14**, 138 (1981).
[9] L. Lehr *et al.*, Science **284**, 635 (1999).
[10] H. A. Gillis and T. I. Quickenden, Can. J. Chem. **79**, 80 (2001).
[11] D. Chakarov and B. Kasemo, Phys. Rev. Lett. **81**, 5181 (1998).
[12] Q. B. Lu and L. Sanche, Phys. Rev. B **63**, 153403 (2001).
[13] E. Knoesel, A. Hotzel, and M. Wolf, Phys. Rev. B **57**, 12812 (1998).
[14] G. Held and D. Menzel, Surf. Sci. **327**, 301 (1995).
[15] R. S. Smith and B. D. Kay, Nature (London) **398**, 788 (1999).
[16] C. Gahl *et al.*, Surf. Sci. (to be published).
[17] M. Wolf, E. Knoesel, and T. Hertel, Phys. Rev. B **54**, R5295 (1996).
[18] N.-H. Ge *et al.*, Science **279**, 202 (1998).
[19] T. Shibaguchi, H. Onuki, and R. Onaka, J. Phys. Soc. Jpn. **42**, 152 (1977), E_{gap} taken at 50% threshold.
[20] M. A. Henderson, Surf. Sci. Rep. **46**, 1 (2002).
[21] A direct excitation process from the extended metal states to the localized states in the ice is unlikely due to the small wave function overlap.
[22] R. A. Marcus and N. Sutin, Biochim. Biophys. Acta **811**, 265 (1985).
[23] C. Gahl *et al.* (to be published).
[24] S. Lee *et al.*, Phys. Rev. Lett. **79**, 2038 (1997).